# Simultaneous amplitude-contrast and quantitative phase-contrast microscopy by numerical reconstruction of Fresnel off-axis holograms

Etienne Cuche, Pierre Marquet, and Christian Depeursinge

We present a digital method for holographic microscopy involving a CCD camera as a recording device. Off-axis holograms recorded with a magnified image of microscopic objects are numerically reconstructed in amplitude and phase by calculation of scalar diffraction in the Fresnel approximation. For phase-contrast imaging the reconstruction method involves the computation of a digital replica of the reference wave. A digital method for the correction of the phase aberrations is presented. We present a detailed description of the reconstruction procedure and show that the transverse resolution is equal to the diffraction limit of the imaging system. © 1999 Optical Society of America

*OCIS codes:* 090.0090, 110.0180, 040.1520, 350.5030, 090.1000.

## 1. Introduction

The idea of reconstructing a hologram with a computer was proposed for the first time more than 30 years ago by Goodman and Laurence[1] and by Kronrod *et al.*[2] At that time the main drawbacks of this numerical approach of holography were the insufficient performance of computers and the lack of adequate devices for digital image acquisition. Today these handicaps have been suppressed, and digital holography can be performed efficiently and inexpensively with a charged-coupled device (CCD) camera for hologram recording and a personal computer for the reconstruction.

In the past ten years digital holography has been applied in various configurations. Haddad *et al.*[3] and Boyer *et al.*[4] reported an application in Fourier-transform holography for biomedical microscopy. A numerical method for the reconstruction of Fresnel holograms recorded with a CCD camera was reported for the first time by Schnars and Jüptner,[5] and similar techniques have been applied in various domains such as position measurement,[6] endoscopy,[7] light-in-flight observation,[8] and optical coherence tomography.[9,10] A method that uses phase-shifting interferometry has also been proposed for in-line holography.[11,12] All the above-mentioned studies concern amplitude-contrast imaging for which only the intensity of the reconstructed optical field is considered. An application of digital holography to hologram interferometry[13,14] has demonstrated the ability of the technique to measure a phase difference between two different states of the object. However, as presented in Refs. 13 and 14, the method cannot be used for the reconstruction of a phase-contrast image on the basis of a single hologram.

In a previous study[15] Cuche *et al.*. demonstrated that phase reconstruction is possible by multiplication of the hologram with a computed replica of the reference wave. It was also demonstrated that the obtained phase contrast is quantitative and can be used directly for applications in optical metrology such as surface profilometry in which a resolution approaching 10 nm has been obtained for step height measurement. Attractive features of this new imaging technique are the high acquisition rate (video frequency) and the high reconstruction rate (~1 Hz), the ability to reconstruct simultaneously an amplitude-contrast and a phase-contrast image, and the ability to provide precise quantitative information about the three-dimensional structure of the specimen by computational means with a single hologram acquisition.

In Ref. 15 holograms were recorded with a Michel-

E. Cuche (etienne.cuche@epfl.ch) and C. Depeursinge are with the Institute of Applied Optics, Swiss Federal Institute of Technology, CH-1015 Lausanne, Switzerland. P. Marquet is with the Institute of Physiology, Laboratory of Neurological Research, Department of Neurology, University of Lausanne, CH-1005 Lausanne, Switzerland.

Received 14 April 1999; revised manuscript received 3 August 1999.

0003-6935/99/346994-08$15.00/0

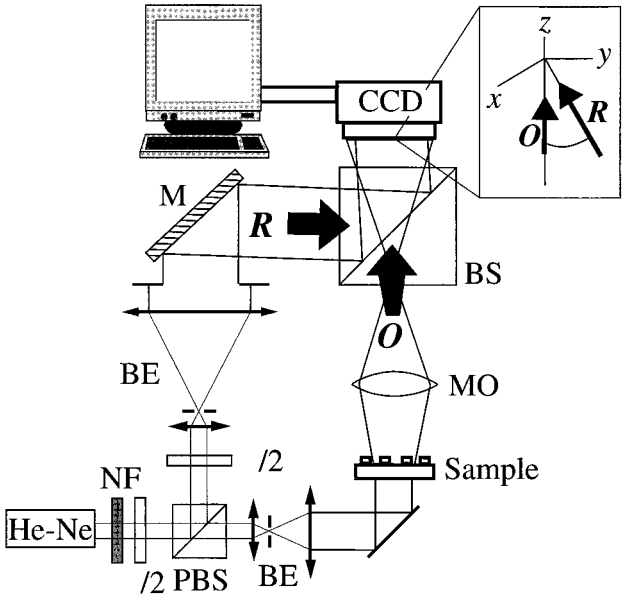


Fig. 1. Schematic of the holographic microscope for transmission imaging. NF, neutral density filter; PBS, polarizing beam splitter; BE, beam expander with spatial filter; λ/2, half-wave plate; M, mirror; BS, beam splitter; **O**, object wave; **R**, reference wave. Inset: detail showing the off-axis geometry at the incidence on the CCD.

son interferometer with an object wave directly reflected by the specimen. In this configuration the transverse resolution was limited to approximately 30 μm. Here we present a new, to our knowledge, configuration designed for microscopic investigations with the same transverse resolution as with classical optical microscopy. The presented instrument could be called a digital holographic microscope and consists of a microscope objective (MO) that produces a magnified image of the sample that is used as an object for the hologram creation. Since a phase aberration is associated with the use of a MO, we also present a digital method that has been developed to correct this aberration.

### 2. Microscope Designs

Two kinds of digital holographic microscope are presented. The first one (Fig. 1) is designed for transmission imaging with transparent samples (e.g., biological cells) and the second one (Fig. 2) for reflection imaging. In both cases the basic architecture is that of a Mach–Zender interferometer. For the present experiments a linearly polarized He–Ne laser (10 mW) is used as a light source. The combination of a neutral density filter, a half-wave plate, and a polarizing beam splitter is used for the adjustment of the intensities in the reference arm and the object arm of the interferometer. In the reference arm a half-wave plate is introduced to obtain parallel polarizations at the exit of the interferometer. In each arm, beam expanders, including pinholes for spatial filtering, are introduced to produce plane waves.

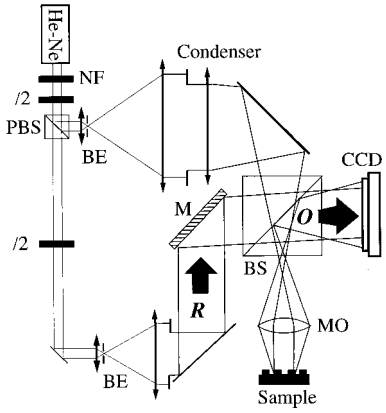


Fig. 2. Schematic of the holographic microscope for reflection imaging. NF, neutral density filter; PBS, polarizing beam splitter; BE, beam expander with spatial filter; λ/2, half-wave plate; M, mirror; BS, beam splitter; **O**, object wave; **R**, reference wave.

For transmission imaging (Fig. 1), the specimen is illuminated by a plane wave and the transmitted light is collected by a MO that produces a wave front called object wave **O**. For reflection imaging (Fig. 2) a lens with a long focal length is inserted between the beam expander and the MO. This lens acts as a condenser, and its position is adjusted to illuminate the sample with a collimated beam. This condenser is important for reflection imaging, because, as explained below, in holographic microscopy the sample may be located near the object focal plane of the MO. If necessary, for example, if a high intensity is desired for the object illumination, a condenser can also be used in the transmission geometry.

At the exit of the interferometer the interference between the object wave **O** and the reference wave **R** creates the hologram intensity,

$$I_H(x, y) = |\mathbf{R}|^2 + |\mathbf{O}|^2 + \mathbf{R}^*\mathbf{O} + \mathbf{R}\mathbf{O}^*, \qquad (1)$$

where $\mathbf{R}^*$ and $\mathbf{O}^*$ denote the complex conjugates of the reference wave and the object wave, respectively. As in Ref. 15 the off-axis geometry is considered. For this reason the mirror that reflects the reference wave (M) is oriented such that the reference wave reaches the CCD camera with a small incidence angle θ (see inset in Fig. 1) with respect to the propagation direction of the object wave.

A digital hologram is recorded by a standard black and white CCD camera (Hitashi Denshi Model KP-M2) and transmitted to a computer by means of a frame grabber card. The digital hologram $I_H(k, l)$ is an array of $N \times N = 512 \times 512$ 8-bit-encoded numbers that results from the two-dimensional sampling of $I_H(x, y)$ by the CCD camera:

$$I_H(k, l) = I_H(x, y)\mathrm{rect}\left(\frac{x}{L}, \frac{y}{L}\right) \times \sum_{k=-N/2}^{N/2} \sum_{l=-N/2}^{N/2} \delta(x - k\Delta x, y - l\Delta y), \qquad (2)$$

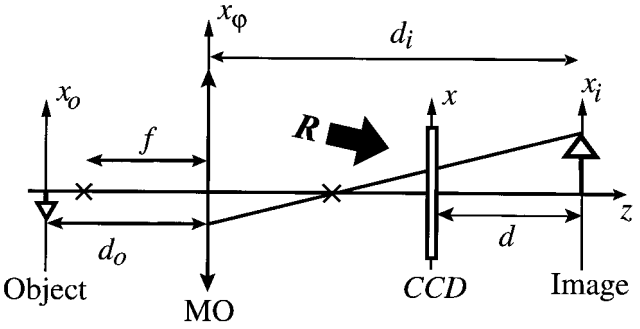


Fig. 3. Configuration for holographic microscopy.

where $k$, $l$ are integers, $L \times L = 4.85\ \text{mm} \times 4.85\ \text{mm}$ is the area of the sensitive chip, and $\Delta x$, $\Delta y$ defines the sampling intervals in the hologram plane (pixel size) $\Delta x = \Delta y = L/N$.

Holographic microscopy has been proposed in various configurations.[16] Here we are working with a geometry including a MO that was proposed for the first time in 1966 by VanLigten and Osterberg.[17] In digital holography a similar approach was used by Schnars *et al.*[14] but with a divergent lens for imaging large objects. As shown in Fig. 3, the optical arrangement in the object arm is an ordinary single-lens imaging system. The MO produces a magnified image of the object, and the hologram plane $0x$ (the CCD plane) is located between the MO and the image plane ($0x_i$), at a distance $d$ from the image. This situation can be considered to be equivalent to a holographic configuration without magnification optics with an object wave emerging directly from the magnified image and not from the object itself. For this reason the term *image holography* is sometimes used to designate this procedure.

Classical microscopy can be achieved with this arrangement by translation of the object or the hologram plane such that the image is focused on the CCD. In this case, if an interference with the reference wave were recorded, it would correspond to a hologram recorded with a zero object–hologram distance. Such a disposition is not appropriate for off-axis holography but is used in interference microscopy where phase-shifting interferometry[18] is applied to obtain the phase information.

A particular case arises when the specimen is located in the object focal plane of the MO. In this case the distance between the image and the MO ($d_i$) is infinite, the hologram is recorded with the Fourier transform of the object field, and the reconstruction can be performed by simple computation of the Fourier transform of the hologram.

### 3. Hologram Reconstruction

The numerical reconstruction method consists basically of calculating the Fresnel diffraction pattern of the hologram. Figure 4 defines the considered

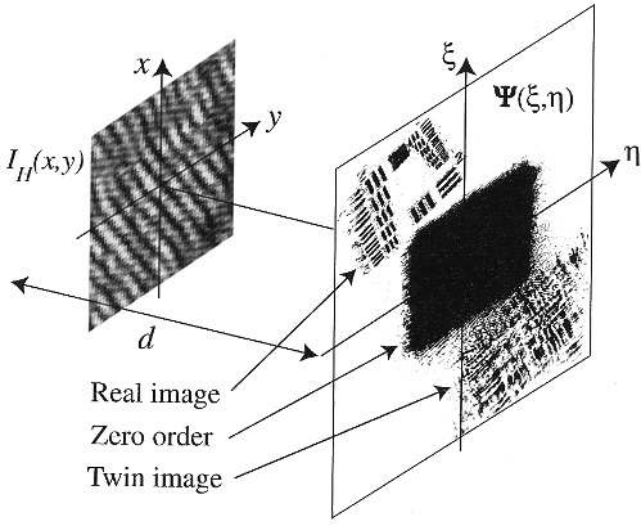


Fig. 4. Geometry for hologram reconstruction. $0xy$, hologram plane; $0\xi\eta$, observation plane; $d$, reconstruction distance; $\Psi(\xi, \eta)$, reconstructed wave front.

geometry. The result of the calculation is an array of complex numbers called reconstructed wave front $\mathbf{\Psi}$, which represents the complex amplitude of the optical field in the observation plane $0\xi\eta$. The distance between the hologram plane $0xy$ and the observation plane is defined by the reconstruction distance $d$. When the hologram is recorded without a MO, $d$ must be equal to the distance (or, more precisely, to the optical path length) between the object and the CCD to obtain in-focus reconstructed images. In holographic microscopy, image focusing occurs when the reconstruction distance is equal to the distance between the CCD and the image during the hologram recording ($d$ in Fig. 3).

In classical holography the reconstruction is carried out by illumination of the hologram intensity with the reference, and the reconstructed wave front is defined as follows:

$$\mathbf{\Psi} = \mathbf{R}I_H = \mathbf{R}|\mathbf{R}|^2 + \mathbf{R}|\mathbf{O}|^2 + |\mathbf{R}|^2\mathbf{O} + \mathbf{R}^2\mathbf{O}^*. \quad (3)$$

The two first terms of Eq. (3) produce a zero order of diffraction, the third term produces a twin image, and the fourth produces a real image. As a consequence of the off-axis geometry these different terms are reconstructed at different locations in the observation plane (see Fig. 4). In classical holography we usually observe the twin image that appears to be emitted by a virtual replica of the object located at its initial position, i.e., behind the hologram. Here, if the reconstruction distance $d$ is positive, the reconstruction takes place in front of the hologram and the real image is in focus. If desired, we can also reconstruct the twin image in focus by taking a negative reconstruction distance ($-d$).

### A. Numerical Calculation of Fresnel Diffraction

In the Fresnel approximation the reconstructed wave front can be written as

$$\mathbf{\Psi}(\xi, \eta) = A \exp\left[\frac{i\pi}{\lambda d}(\xi^2 + \eta^2)\right] \times \iint I_H(x, y)\exp\left[\frac{i\pi}{\lambda d}(x^2 + y^2)\right] \times \exp\left[\frac{i2\pi}{\lambda d}(x\xi + y\eta)\right]\mathrm{d}x\mathrm{d}y, \quad (4)$$

where $\lambda$ is the wavelength, $d$ is the reconstruction distance, and $A = \exp(i2\pi d/\lambda)/(i\lambda d)$ is a complex constant. As presented by Eq. (4), the Fresnel integral can be viewed as a Fourier transform, in the spatial frequencies $\xi/\lambda d$ and $\eta/\lambda d$, of the function

$$I_H(x, y)\exp\left[\frac{i\pi}{\lambda d}(x^2 + y^2)\right]. \quad (5)$$

For rapid numerical calculations a discrete formulation of Eq. (4) involving a two-dimensional fast Fourier transform can be derived directly:

$$\mathbf{\Psi}(m, n) = A \exp\left[\frac{i\pi}{\lambda d}(m^2\Delta\xi^2 + n^2\Delta\eta^2)\right] \times \mathrm{FFT}\left\{I_H(k, l)\exp\left[\frac{i\pi}{\lambda d}(k^2\Delta x^2 + l^2\Delta y^2)\right]\right\}_{m,n}, \quad (6)$$

where $k, l, m, n$ are integers ($-N/2 \le k, l, m, n \le N/2$) and $I_H(k, l)$ is the digital hologram [Eq. (2)]. The values of the sampling intervals in the observation plane ($\Delta\xi$ and $\Delta\eta$) can be deduced directly from the relationship between the sampling intervals in the direct ($0x$) and Fourier ($0\nu$) spaces in discrete Fourier-transform calculations: $\Delta\nu = 1/(N\Delta x)$. Taking into account that in our case the Fourier transform must be calculated in the spatial frequencies $\xi/\lambda d$ and $\eta/\lambda d$, we have

$$\Delta\xi = \Delta\eta = \frac{\lambda d}{N\Delta x} = \frac{\lambda d}{L}, \quad (7)$$

where $L$ is the size of the CCD. In a setup without a MO, as presented, for example, in Refs. 5 and 15, $\Delta\xi$ defines the transverse resolution in the observation plane. For a typical reconstruction distance $d = 30$ cm with a wavelength $\lambda = 633$ nm and a CCD size $L = 5$ mm, the transverse resolution of the imaging system is limited to $\Delta\xi = 38$ $\mu$m. In holographic microscopy $\Delta\xi$ defines the resolution with which the magnified image of the object is reconstructed, and, as shown experimentally in this paper, a transverse resolution equal to the diffraction limit of the MO can be achieved.

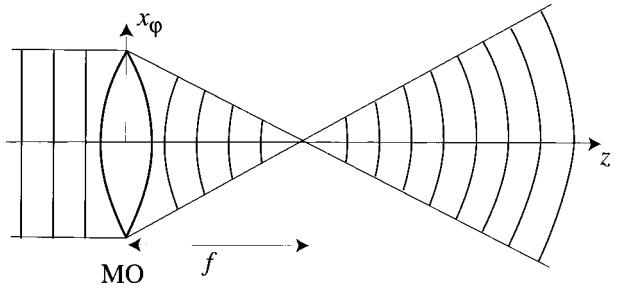


Fig. 5. Schematic of the wave-front deformation by the MO.

### B. Phase-Contrast Imaging

As explained in Ref. 15, for phase-contrast imaging the digital hologram has to be multiplied by a digital reference wave $\mathbf{R}_D$, which must be replica of the experimental reference wave $\mathbf{R}$. In classical holography, the same operation is performed optically when the hologram is illuminated with the reference wave. If we assume that a perfect plane wave is used as reference for hologram recording, $\mathbf{R}_D$ is calculated as follows:

$$\mathbf{R}_D(k, l) = A_R \exp[i(2\pi/\lambda)(k_x k\Delta x + k_y l\Delta y)], \quad (8)$$

where $A_R$ is the amplitude, $\Delta x$ and $\Delta y$ are the sampling intervals in the hologram plane, and $k_x$, $k_y$ are the two components of the wave vector that must be adjusted such that the propagation direction of $\mathbf{R}_D$ matches as closely as possible that of the experimental reference wave.

### C. Digital Correction of the Phase Aberrations

As shown in Fig. 5 the MO produces a curvature of the wave front in the object arm. This deformation affects only the phase of the object wave and does not disturb amplitude-contrast imaging. However, for phase-contrast imaging or, more generally, in any interferometric system, this phase aberration must corrected.

In interference microscopy[18] this problem is solved experimentally by insertion of the same MO in the reference arm, at equal distance from the exit of the interferometer. This arrangement, called the Linnik interferometer, requires that, if any change has to be made in the object arm, then the same change must be precisely reproduced in the reference arm such that the interference occurs between similarly deformed wave fronts. An other possibility (Mirrau interferometry) consists of magnifying the interference pattern. However, it is difficult to achieve high-resolution imaging with this technique, because a miniaturized interferometer must be inserted between the sample and the MO. As reported by Sun and Arons,[19] it is also possible to design a phase-compensation lens.

Here we propose a digital method that allows us to perform the correction by multiplication of the reconstructed wave front with the computed complex conjugate of the phase aberration. Since the hologram is recorded with an image of the object, the problem is

to describe the phase deformation produced by the MO in the image plane. If we assume a monochromatic illumination, the relation between the optical fields $\mathbf{U}_i(x_i, y_i)$ in the image plane and $\mathbf{U}_o(x_o, Iy_o)$ in the object plane can be described as follows:

$$\mathbf{U}_i(x_i, y_i) = \iint \mathbf{h}(x_i, y_i; x_o, y_o)\mathbf{U}(x_o, y_o)\mathrm{d}x_o\mathrm{d}y_o, \quad (9)$$

where $\mathbf{h}(x_i, y_i; x_o, y_o)$ is the amplitude point-spread function. If the image plane and the object plane form an object–image relation,

$$\frac{1}{d_i} + \frac{1}{d_o} = \frac{1}{f}, \quad (10)$$

$\mathbf{h}(x_i, y_i; x_o, y_o)$ can be written as follows (in two dimensions, $x$ and $z$, for simplicity)[20]:

$$\mathbf{h}(x_i, x_o) = C \exp\left(\frac{i\pi}{\lambda d_i} x_i^2\right)\exp\left(\frac{i\pi}{\lambda d_o} x_o^2\right) \times \int P(x_\phi)\exp\left[\frac{-i2\pi}{\lambda}\left(\frac{x_o}{d_o} + \frac{x_i}{d_i}\right)x_\phi\right]\mathrm{d}x_\phi, \quad (11)$$

where $0x_\phi$ is the coordinate of the MO plane, $P(x_\phi)$ is the pupil function of the MO, and $C$ is a complex constant. Under the assumption of a perfect imaging system of magnification $M = d_i/d_o$, for which a point of coordinates $(x_o, y_o)$ in the object plane becomes a point of coordinates $(x_i = -Mx_o, y_i = -My_o)$ in the image plane, the integral in Eq. (11) can be approximate by a Dirac δ function. If we replace $x_o$ with $-x_i d_o/d_i$ in the quadratic phase term preceding the integral, we can write

$$\mathbf{h}(x_i, y_i; x_o, y_o) \cong C \exp\left[\frac{i\pi}{\lambda d_i}\left(1 + \frac{d_o}{d_i}\right)(x_i^2 + y_i^2)\right] \times \delta(x_i + Mx_o, y_i + My_o). \quad (12)$$

In other words, relation (12) means that the image field is a magnified replica of the object field multiplied by a paraboloidal phase term. For our purpose here it also means that the phase aberration can be corrected by multiplication of the reconstructed wave front with the complex conjugate of the phase term that precedes the δ function in relation (12). Therefore an array of complex numbers called digital phase mask $\mathbf{\Phi}(m, n)$ is calculated as follows:

$$\mathbf{\Phi}(m, n) = \exp\left[\frac{-i\pi}{\lambda D}(m^2\Delta\xi^2 + n^2\Delta\eta^2)\right], \quad (13)$$

where $D$ is a parameter that must be adjusted to compensated the wave-front curvature. In accordance with relation (12) we have

$$\frac{1}{D} = \frac{1}{d_i}\left(1 + \frac{d_o}{d_i}\right). \quad (14)$$

Even if this development should appear simplistic with respect to the general theory of optical aberrations, we show here that high-quality phase-contrast images can be obtained with this model. The use of more sophisticated models can be envisaged to describe the optical aberrations (in amplitude and phase) to perform a more accurate digital correction.

Finally, taking into account the developments made in Subsections 3.A [Eqs. (6) and (7)], 3.B, and 3.C, the complete expression of the reconstruction algorithm becomes

$$\mathbf{\Psi}(m, n) = A\mathbf{\Phi}(m, n)\exp\left[\frac{i\pi}{\lambda d}(m^2\Delta\xi^2 + n^2\Delta\eta^2)\right] \times \mathrm{FFT}\left\{\mathbf{R}_D(k, l)I_H(k, l) \times \exp\left[\frac{i\pi}{\lambda d}(k^2\Delta x^2 + l^2\Delta y^2)\right]\right\}_{m,n}. \quad (15)$$

Since $\mathbf{\Psi}(m, n)$ is an array of complex numbers, we can obtain an amplitude-contrast image by calculating the intensity,

$$I(m, n) = \mathrm{Re}[\mathbf{\Psi}(m, n)]^2 + \mathrm{Im}[\mathbf{\Psi}(m, n)]^2, \quad (16)$$

and a phase-contrast image by calculating the argument,

$$\phi(m, n) = \arctan\left\{\frac{\mathrm{Im}[\mathbf{\Psi}(m, n)]}{\mathrm{Re}[\mathbf{\Psi}(m, n)]}\right\}. \quad (17)$$

The reconstruction algorithm [Eq. (15)] involves four constants called reconstruction parameters: $d$, the reconstruction distance; $k_x$ and $k_y$ for the calculation of the digital reference wave [Eq. (8)]; and $D$ for the calculation of the digital phase mask [Eq. (13)]. These reconstruction parameters represent physical quantities (distances and angles) and could be measured experimentally. However, their values must be defined with such a high precision that it is more efficient to adjust them digitally. In Subsection 4.B we describe the procedure used for the adjustment of the reconstruction parameters.

## 4. Results and Discussion

### A. Typical Example

Figure 6 presents a digital hologram recorded with the experimental setup presented in Fig. 2, with a MO of magnification $M = 40$ and of numerical aperture N.A. = 0.65. To study the transverse resolution limit of the system, a test target [USAF (U.S. Air Force) 1950] was used as a sample. This standard test object contains horizontal and vertical three-bar patterns in the form of a reflecting chromium coating set on a glass substrate.

We can see in Fig. 6 that the hologram appears as a pattern of interference fringes. These fringes are curved because of the phase aberration produced by the MO (Fig. 5) and are not concentric with respect to

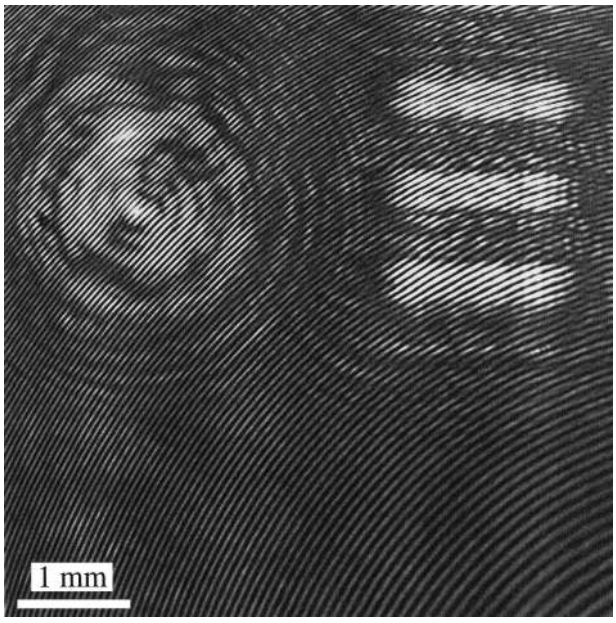


Fig. 6. Digital hologram recorded by the CCD camera.

the center of the image as a consequence of the off-axis geometry.

The corresponding reconstructed amplitude- and phase-contrast images are presented in Figs. 7(a) and 7(b), respectively. These images do not represent the entire area of the observation plane but only a selected region of interest (200 × 120 pixels) containing the real image. The reconstructed three-bar pattern is the sixth element of group 6 of the USAF test target and corresponds to a spatial frequency of 114 lp/mm (line pairs/mm). Because small details of these elements are clearly observable, we can conclude that a transverse resolution smaller than 1 μm has been achieved. This result agrees with the predicted resolution limit of the MO as calculated according to the Abbe criterion ($0.61\lambda/\text{N.A.} \cong 0.59$ μm).

Figure 4(c), which presents a three-dimensional perspective of the reconstructed phase distribution, is shown here to illustrate the fact that the phase-contrast image provides information about the three-dimensional structures of the sample. In Ref. 15 an experiment performed with a surface of homogenous optical properties demonstrated that phase changes corresponding to less than 10 nm can be measured on the basis of the reconstructed phase-contrast image.

It is also important to note that the obtained phase values are restricted to the $[-\pi, \pi]$ interval. If the sample produces phase variations higher than the wavelength, phase-unwrapping methods must be applied to reconstruct the topography.

### B. Adjustment of the Reconstruction Parameters

As explained in Section 3, the reconstruction algorithm [Eq. (15)] involves four constants called reconstruction parameters. The values of these constants are fixed for a given experimental configuration but must be modified if the reference-wave orientation is changed or if the sample is translated along the optical axis *0z*. In the current section we describe how the reconstruction parameters can be adjusted by showing examples of images that have been reconstructed for different values of these parameters.

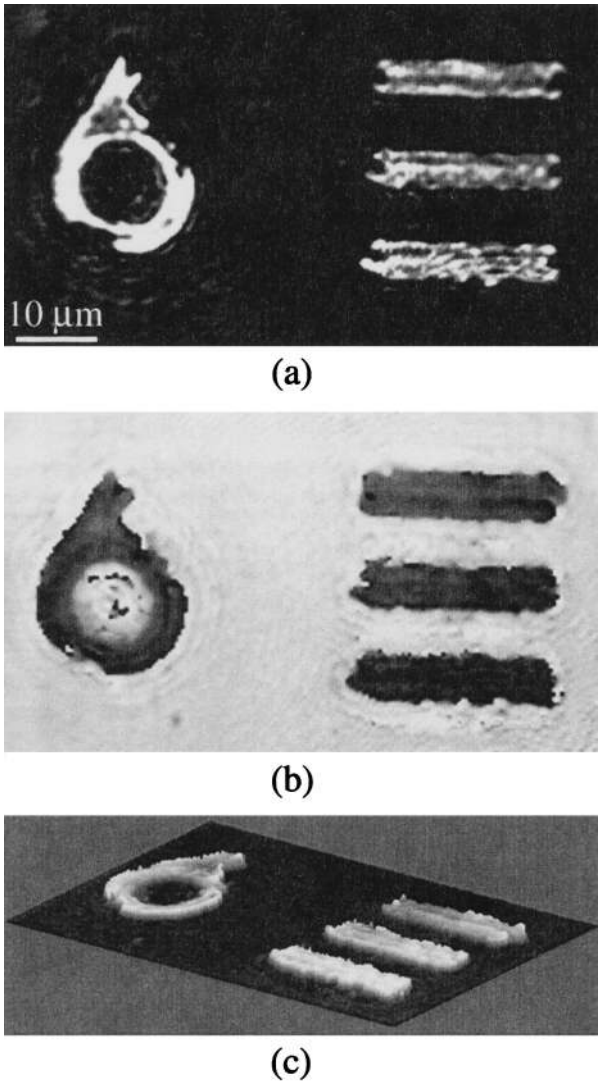


Fig. 7. Reconstructed images corresponding to the hologram presented in Fig. 6. (a) Amplitude-contrast image, (b) phase-contrast image, (c) the reconstructed phase distribution presented in a three-dimensional perspective.

The first parameter that has to be adjusted is the reconstruction distance $d$. In Fig. 8, which presents three amplitude-contrast images of the USAF test target obtained for different values of $d$, we can see that the reconstruction distance is related to image focusing. The procedure for the adjustment of $d$ can be considered to be the digital counterpart of image focusing in classical microscopy in which the same operation is performed by translation of the sample along the optical axis. Autofocus methods can be used to adjust $d$ automatically. The images presented in Fig. 8 have been reconstructed from a hologram recorded by use of the experimental setup presented in Fig. 2 with a MO of numerical aperture

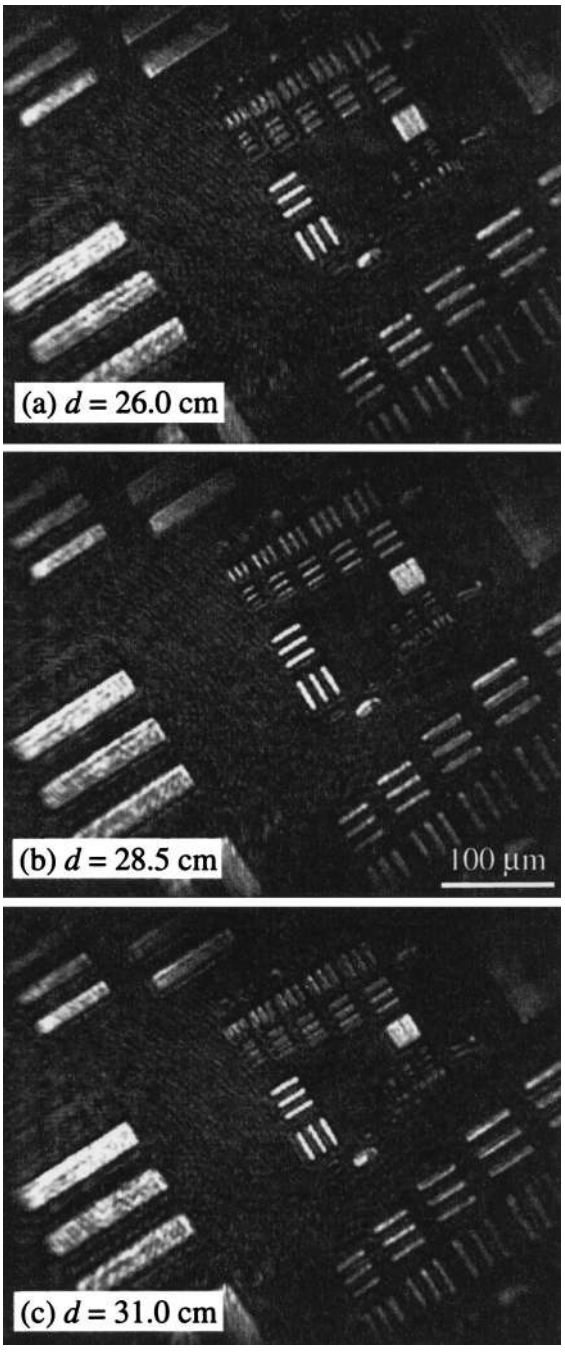


Fig. 8. Amplitude-contrast images obtained for different values of the reconstruction distance $d$. (a) Out of focus image ($d$ too short), (b) in-focus image, (c) out of focus image ($d$ too long).

N.A. = 0.1. In the in-focus image of Fig. 8(b), we can see that the sixth element of group 6 (114 lp/mm) is the smallest resolved three-bar pattern. We can then conclude that a transverse resolution approximately equal to the diffraction limit of the MO ($0.61\lambda$/N.A. $\cong$ 3.86 μm) has been achieved. This result was verified for other MO's with higher numerical apertures.

For the reconstruction of phase-contrast images three other reconstruction parameters have to be adjusted: $k_x$ and $k_y$ for the calculation of the digital

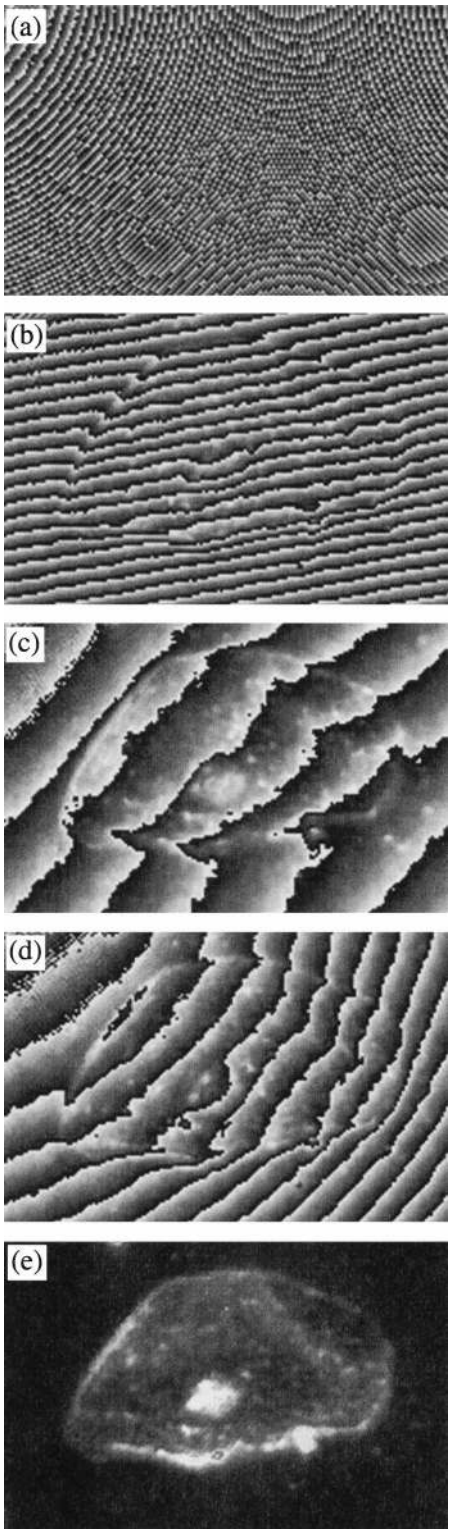


Fig. 9. Phase-contrast images obtained for different values of $k_x$, $k_y$, and $D$. (a) Without digital reference wave and without digital phase mask ($k_x = 0.0$, $k_y = 0.0$, no phase mask), (b) without digital reference wave and with proper digital phase mask ($k_x = 0.0$, $k_y = 0.0$, $D = 0.258$), (c) with proper digital phase mask and wrong digital reference wave ($k_x = 9.0 \times 10^{-3}$, $k_y = 1.0 \times 10^{-3}$, $D = 0.258$), (d) with proper digital reference wave and wrong digital phase mask ($k_x = 11.08 \times 10^{-3}$, $k_y = 2.05\ 10^{-3}$, $D = 0.240$), (e) with proper digital reference wave and proper digital phase mask ($k_x = 11.08 \times 10^{-3}$, $k_y = 2.05\ 10^{-3}$, $D = 0.258$).

reference wave and $D$ for the calculation of the digital phase mask. Figure 9 shows five phase-contrast images of an epithelial cell obtained for different values of $k_x$, $k_y$, and $D$. On one hand, Fig. 9(a) presents the extreme case of an image obtained without a phase mask and without a digital reference wave ($k_x = k_y = 0$). On the other hand, Fig. 9(e) presents the case of a phase-contrast image obtained with properly adjusted reconstruction parameters. Figure 9(b) presents an image obtained without a digital reference wave but with the appropriate digital phase mask ($D$ correctly adjusted). We can see that straight fringes with a fixed orientation appear in Fig. 9(b). These fringes indicate jumps of the phase values between $-\pi$ and $+\pi$ that appear when a phase difference equal to a multiple of $2\pi$ exists between the wave fronts of the digital reference wave $\mathbf{R}_D$ and the wave fronts of the experimental reference wave $\mathbf{R}$. As illustrated by Fig. 9(c), the procedure for the adjustment of $k_x$ and $k_y$ consists of enlarging the space between these fringes until they completely disappear. As shown in Fig. 9(d), if the digital reference wave is correctly defined but the $D$ value is slightly modified, the digital phase mask does not properly correct the phase aberrations of the MO and curved fringes appear on the reconstructed image. The procedure for the adjustment of $D$ consists of removing the fringe curvature.

A fine adjustment of $k_x$, $k_y$, and $D$ can be performed in the absence of fringes by removal of residual gradients or curvature of the reconstructed phase distribution in some area of the image where a constant phase is presumed. In Fig. 9, for example, the reconstruction parameters have been adjusted to obtain a constant phase distribution outside the cell, which was placed on a glass plate.

## 5. Conclusions

A digital holographic microscope that is capable of simultaneous amplitude- and phase-contrast imaging has been constructed and tested. It has been established that the transverse resolution of this new, to our knowledge, imaging technique is equal to the diffraction limit of the imaging system as is true with classical optical microscopy. Image focusing, phase reconstruction, and correction of the phase aberrations are performed digitally and require the adjustment of four reconstruction parameters. An attractive feature of this instrument is that precise quantitative information about the three-dimensional structure of the sample can be obtained on the basis of only one hologram, which can be acquired at the video frequency. Applications in both biological and materials science microscopy are expected.

This study was supported by Swiss National Fund for Scientific Research grant 20-49628.96. The authors thank P. Dahlgren, P. Poscio, and D. Beghuin for their contributions.

## References

1. J. W. Goodman and R. W. Lawrence, "Digital image formation from electronically detected holograms," Appl. Phys. Lett. **11,** 77–79 (1967).
2. M. A. Kronrod, N. S. Merzlyakov, and L. P. Yaroslavskii, "Reconstruction of a hologram with a computer," Sov. Phys. Tech. Phys. **17,** 333–334 (1972).
3. W. S. Haddad, D. Cullen, J. C. Solem, J. W. Longworth, A. McPherson, K. Boyer, and C. K. Rhodes, "Fourier-transform holographic microscope," Appl. Opt. **31,** 4973–4978 (1992).
4. K. Boyer, J. C. Solem, J. W. Longworth, A. B. Borisov, and C. K. Rhodes, "Biomedical three-dimensional holographic microimaging at visible, ultraviolet and X-ray wavelength," Nat. Med. (N.Y.) **2,** 939–941 (1996).
5. U. Schnars and W. Jüptner, "Direct recording of holograms by a CCD target and numerical reconstruction," Appl. Opt. **33,** 179–181 (1994).
6. K. Yoshinori, U. Hiroaki, T. Kenji, H. Okamoto, and E. Shimizu, "Three-dimensional shape measurement using images reconstructed by the computer from a hologram," in *Practical Holography VIII*, S. A. Benton, ed., Proc. SPIE **2716,** 272–282 (1994).
7. O. Coquoz, R. Conde, F. Taleblou, and C. Depeursinge, "Performances of endoscopic holography with a multicore optical fiber," Appl. Opt. **34,** 7186–7193 (1995).
8. J. Pomarico, U. Schnars, H.-J. Hartmann, and W. Jüptner, "Digital recording and numerical reconstruction of holograms: a new method for displaying light in flight," Appl. Opt. **34,** 8095–8099 (1995).
9. E. Cuche, P. Poscio, and C. Depeursinge, "Optical tomography at the microscopic scale by means of a numerical low coherence holographic technique," in *Optical and Imaging Techniques for Biomonitoring II*, H. J. Foth, R. Marchesini, and H. Pobielska, eds., Proc. SPIE **2927,** 61–66 (1996).
10. E. Cuche, P. Poscio, and C. Depeursinge, "Tomographie optique par une technique d'holographie numérique en faible cohérence," J. Opt. (Paris) **28,** 260–264 (1997).
11. I. Yamaguchi and T. Zhang, "Phase-shifting digital holography," Opt. Lett. **22,** 1268–1270 (1997).
12. T. Zhang and I. Yamaguchi, "Three-dimensional microscopy with phase-shifting digital holography," Opt. Lett. **23,** 1221–1223 (1998).
13. U. Schnars, "Direct phase determination in hologram interferometry with use of digitally recorded holograms," J. Opt. Soc. Am. A **11,** 2011–2015 (1994).
14. U. Schnars, T. M. Kreis, and W. P. O. Jüptner, "Digital recording and numerical reconstruction of holograms: reduction of the spatial frequency spectrum," Opt. Eng. **35,** 977–982 (1996).
15. E. Cuche, F. Bevilacqua, and C. Depeursinge, "Digital holography for quantitative phase-contrast imaging," Opt. Lett. **24,** 291–293 (1999).
16. See, for example, M. Pluta, "Holographic microscopy," in *Advances in Optical and Electron Microscopy,* R. Barer and V. E. Cosslett, eds. (Academic, London, 1987), Vol. 10, pp. 99–213.
17. R. F. VanLigten and H. Osterberg, "Holographic microscopy," Nature **211,** 282–283 (1966).
18. J. E. Greivenkamp and J. H. Brunning, "Phase shifting interferometry"; K. Creath and A. Morales, "Contact and noncontact profilers," in *Optical Shop Testing*, 2nd ed., Wiley Series in Pure and Applied Optics, D. Malacara, ed. (Wiley, New York, 1992), Chaps. 14 and 17.
19. P. C. Sun and E. Arons, "Nonscanning confocal ranging system," Appl. Opt. **34,** 1254–1261 (1995).
20. J. W. Goodman, *Introduction to Fourier Optics* (McGraw-Hill, San Francisco, Calif., 1968), Chap. 5.